MULTISCALE MODELLING OF DEFORMATION PROCESSES OF NODULAR CAST IRON

Tomislav Lesičar, Zdenko Tonković, Jurica Sorić, Predrag Čanžar

Faculty of Mechanical Engineering and Naval Architecture, University of Zagreb,

Ivana Lučića 5, 10000 Zagreb, Croatia, tomislav.lesicar@fsb.hr, ztonkov@fsb.hr, jurica.soric@fsb.hr, predrag.canzar@fsb.hr

1. Introduction

In recent years, a special attention has been paid to investigate relations between the microstructure and mechanical properties of materials since almost all materials used in engineering are micro-heterogeneous. It is well-known that the classical continuum mechanics does not consider structural effects in the material at the micro-level. To overcome this problem, multiscale techniques have been developed for modelling of macroscopic behaviour of heterogeneous materials where the results obtained by the analysis of a representative volume element (RVE) (micro-level) are used as an input to the continuum model (macro-level) [1]. To solve the problem at the micro-level the finite element (FE) method is mostly applied [1], [2], [3].

This paper provides an overview of the studies that are performed in order to investigate the influence of the size and distribution of graphite nodules in a ferrite matrix on the mechanical behaviour of the ductile cast iron EN-GJS-400-18-LT [4]. To obtain more accurate results second order homogenization algorithm is applied, as shown in [1]. The algorithm is derived for the plane stress and plane strain state assuming the elastoplastic behaviour of the material constituents. For the computational homogenization purposes on macro-level, a strain gradient finite element with C^1 continuity is used, originally proposed in [5][4] for plate bending problems. The finite element and computational homogenization algorithm derived are implemented into the FE program ABAQUS/Standard using user-defined subroutines [6].

2. Second-order computational homogenization algorithm

Fig. 1 presents the scheme of the multiscale computational algorithm based on the second-order homogenization technique. The left side of the figure shows the macro-level model, while the right side depicts a representative volume element (RVE) on the micro-level. Herein, the RVE is discretized by the first-order quadrilateral four-node finite elements, while the strain gradient three-node triangular elements are used on the macro-level. The RVE is the smallest material volume that contains all essential information about microstructure, and therefore, the RVE has to be defined as the statistically representative sample of the material on the micro structural level. The computational homogenization algorithm based on the linear displacement boundary condition on the RVE, consists of the steps shown in Table 1.

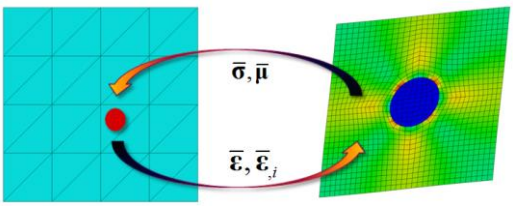

Figure 1. Multi-scale computational scheme

As may be seen from the Table 1, the micro-level analysis is performed using the macroscopic strain $\bar{\boldsymbol{\varepsilon}}$, and the strain gradient $\bar{\boldsymbol{\varepsilon}}_{,i}$, which are then transformed into the boundary nodal displacements of the RVE. Thereafter, the macroscopic stress $\bar{\boldsymbol{\sigma}}$, the double stress $\bar{\boldsymbol{\mu}}$ and the tangent stiffness $\bar{\mathbf{C}}$ are obtained from the solution of the RVE boundary value problem at each macro-level integration point by averaging over the RVE.

3. FE formulation and verification

This paper presents the derivation of a three-node triangular finite element for the plane elasticity with C^1 continuity according to [7], needed for second homogenization purposes. The element formulation is based on the

Aifantis gradient elasticity theory, which is a special case of Mindlin's Form II strain gradient theory.

Table 1. Computational homogenization algorithm

1. Define strain increment $\Delta\bar{\boldsymbol{\varepsilon}}$, and strain gradient $\Delta\bar{\boldsymbol{\varepsilon}}_{,i}$, at the macro level.
2. Calculation of the displacement increment at RVE boundary nodes.
3. Solution of the RVE boundary value problem.
4. Calculation of the macroscopic stress $\bar{\boldsymbol{\sigma}}$, the double stress $\bar{\boldsymbol{\mu}}$, and the tangent stiffness $\bar{\mathbf{C}}$.

3.1 Gradient Elasticity Formulation

According to Form II of Mindlin's theory, the strain energy density function depending on the deformation and the deformation gradient may be written as

$$W = W\left(\varepsilon_{ij}, \varepsilon_{ij,k}\right), \tag{1}$$

where the deformation is expressed by well-known relation $\varepsilon_{ij} = \frac{1}{2}\left(u_{i,j} + u_{j,i}\right)$. Using Eq. (1), the variation of the strain energy density function yields the expression

$$\delta W = \frac{\partial W}{\partial \varepsilon_{ij}}\delta\varepsilon_{ij} + \frac{\partial W}{\partial \varepsilon_{ij,k}}\delta\varepsilon_{ij,k}, \tag{2}$$

which may be rewritten in the following form

$$\delta W = \sigma_{ij}\delta\varepsilon_{ij} + \mu_{kij}\delta\varepsilon_{ij,k}. \tag{3}$$

In the last equation, σ_{ij} is the stress tensor, while μ_{kij} denotes the double stress tensor. By splitting deformation tensor in expression (3) into its symmetric and antisymmetric parts and after some suitable formulae manipulations, the following relation for the strain energy density can be obtained

$$\begin{aligned}\delta W = &\left[\left(\sigma_{ji} - \mu_{kji,k}\right)\delta u_i\right]_{,j} \\ &-\left(\sigma_{ji,j} - \mu_{kji,kj}\right)\delta u_i + \left(\mu_{kji}\delta u_{i,j}\right)_{,k}.\end{aligned} \tag{4}$$

3.2 Weak form of the principle of virtual work

The variation of the work done by the internal forces is defined as

$$\delta W_I = \int_V \delta W dV. \tag{5}$$

Inserting equation (4) into (5) and after applying Gauss theorem, the variation of the internal forces takes the following form

$$\begin{aligned}\delta W_I = &\int_S n_j\left(\sigma_{ji} - \mu_{kji,k}\right)\delta u_i dS \\ &-\int_V \left(\sigma_{ji,j} - \mu_{kji,kj}\right)\delta u_i dV \\ &+\int_S n_k\mu_{kji}\delta u_{i,j} dS.\end{aligned} \tag{6}$$

By decomposition of displacement variation in the last term of Eq. (6) into the surface and normal gradients, this equation can be transformed into the following form

$$\begin{aligned}\delta W_I = &\int_S \Big[n_j\left(\sigma_{ji} - \mu_{kji,k}\right) \\ &-\mathrm{D}_j\left(n_k\mu_{kji}\right) + \left(\mathrm{D}_l n_l\right) n_j n_k \mu_{kji}\Big]\delta u_i dS \\ &-\int_V \left(\sigma_{ji,j} - \mu_{kji,kj}\right)\delta u_i dV + \int_S n_k\mu_{kji} n_j \mathrm{D}\delta u_i dS,\end{aligned} \tag{7}$$

with $\mathrm{D}_j = \left(\delta_{jl} - n_j n_l\right)\partial_l$ and $\mathrm{D} = n_l\partial_l$. The variation of the external work is given as

$$\delta W_E = \int_S t_i\delta u_i dS + \int_S \tau_i \mathrm{D}\delta u_i dS, \tag{8}$$

where t_i and τ_i are the traction and double surface traction, respectively. The principle of virtual work $\left(\delta W_I = \delta W_E\right)$, for any admissible variation of δu_i and $\mathrm{D}\delta u_i$ gives the following equilibrium equation

$$\sigma_{ji,j} - \mu_{kji,k} = 0, \tag{9}$$

where

$$\begin{aligned}t_i = &n_j\left(\sigma_{ji} - \mu_{kji,k}\right) - \mathrm{D}_j\left(n_k\mu_{kji}\right) \\ &+\left(\mathrm{D}_l n_l\right) n_j n_k \mu_{kji}, \\ \tau_i = &\, n_j n_k \mu_{kji}.\end{aligned} \tag{10}$$

Using the definition of the effective stress in the form

$$\tilde{\sigma}_{ji} = \sigma_{ji} - \mu_{kji,k}, \tag{11}$$

the equilibrium equation becomes

$$\tilde{\sigma}_{ji,j} = 0, \tag{12}$$

with σ_{ji} defined as the local stress.

3.3 Aifantis constitutive relation

According to Eq. (1), the general form of the strain energy density function for an isotropic, gradient-dependent elastic material is expressed by the following relation

$$\tilde{W} = \frac{1}{2}\lambda\varepsilon_{ii}\varepsilon_{jj} + \mu\varepsilon_{ij}\varepsilon_{ij} + c_1\varepsilon_{ij,k}\varepsilon_{ik,k} + c_2\varepsilon_{ii,k}\varepsilon_{kj,j} + c_3\varepsilon_{ii,k}\varepsilon_{jj,k} + c_4\varepsilon_{ij,k}\varepsilon_{ij,k} + c_5\varepsilon_{ij,k}\varepsilon_{kj,i}. \quad (13)$$

In the special case of Aifantis gradient elasticity only the coefficients c_3 and c_4 are different from zero, so the elastic strain energy density may be reduced to

$$W = \frac{1}{2}\lambda\varepsilon_{ii}\varepsilon_{jj} + \mu\varepsilon_{ij}\varepsilon_{ij} + l^2\left(\underbrace{\frac{1}{2}\lambda\varepsilon_{ii,k}\varepsilon_{jj,k}}_{c_3} + \underbrace{\mu\varepsilon_{ij,k}\varepsilon_{ij,k}}_{c_4}\right). \quad (14)$$

where l is a material parameter with the dimension of length related to the microstructure. Using relation (14) the following quantities are defined

$$\sigma_{ij} = \frac{\partial W}{\partial \varepsilon_{ij}} = \lambda\varepsilon_{pp}\delta_{ij} + 2\mu\varepsilon_{ij}, \qquad \mu_{kji} = \frac{\partial W}{\partial \varepsilon_{ij,k}} = l^2\left(\lambda\varepsilon_{pp}\delta_{ij} + 2\mu\varepsilon_{ij}\right)_{,k}. \quad (15)$$

It is worthy of note that σ_{ij} and μ_{kji} are conjugate quantities to ε_{ij} and $\varepsilon_{ij,k}$, respectively. Furthermore, inserting Eq. (15) into the expression for the effective stress (11) gives the relation

$$\tilde{\sigma}_{ij} = \lambda\varepsilon_{pp}\delta_{ij} + 2\mu\varepsilon_{ij} - l^2\left(\lambda\varepsilon_{pp}\delta_{ij} + 2\mu\varepsilon_{ij},\right)_{,kk}. \quad (16)$$

3.4 FE implementation

The above described relations have been implemented into the finite element formulation, where the higher order finite element for plate bending problems [5] has been adapted for 2D problems [7]. The element displacement field is approximated by the complete fifth order polynomial

$$u = a_1 + a_2x + a_3y + a_4x^2 + a_5xy + a_6y^2 + a_7x^3 + a_8x^2y + a_9xy^2 + a_{10}y^3 + a_{11}x^4 + a_{12}x^3y + a_{13}x^2y^2 + a_{14}xy^3 + a_{15}y^4 + a_{16}x^5 + a_{17}x^4y + a_{18}x^3y^2 + a_{19}x^2y^3 + a_{20}xy^4 + a_{21}y^5. \quad (17)$$

The 2D strain gradient triangular FE shown in Fig. 2 has three nodes with six nodal degrees of freedom for each displacement component (the displacement, two first and three second derivatives).

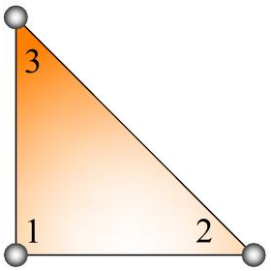

Figure 2. Strain gradient triangular finite element

The element is labeled as C1PS3 by its properties (C^1 continuity, plain stress, 3 nodes). The nodal degrees of freedom are

$$\mathbf{v}_i^T = \begin{pmatrix} u & u_{,x} & u_{,y} & u_{,xx} & u_{,xy} & u_{yy} \\ v & v_{,x} & v_{,y} & v_{,xx} & v_{,xy} & v_{,yy} \end{pmatrix}, \quad (18)$$

where the node number i takes the values 1, 2 and 3. Furthermore, the element displacement vector is given by

$$\mathbf{u} = \mathbf{N}\mathbf{v}, \quad (19)$$

where $\mathbf{N}$ is the shape function matrix in the form

$$\mathbf{N} = \begin{pmatrix} N_1 \ldots N_6 & \mathbf{0} & N_7 \ldots N_{12} \\ \mathbf{0} & N_1 \ldots N_6 & \mathbf{0} \\ \mathbf{0} & N_{13} \ldots N_{18} & \mathbf{0} \\ N_7 \ldots N_{12} & \mathbf{0} & N_{13} \ldots N_{18} \end{pmatrix}. \quad (20)$$

To define the polynomial coefficients $a_1 \ldots a_{21}$ in Eq. (17), 21 equation is required. It is easy to verify that only 18 equations can be defined, which means that system of equations is three times undefined. Therefore, the additional three equations should be derived using the condition that the normal derivative of displacements along the element edges vary as a cubic polynomial [8]. Then, the shape function matrix defined by Eq. (20) can be derived as presented in [5] and [7].

By means of Eqs. (3), (5) and (8) the principle of virtual work may be written as

$$\int_V \sigma_{ij}\delta\varepsilon_{ij}dV + l^2\int_V \mu_{kji}\delta\varepsilon_{ij,k}dV = \int_S t_i\delta u_i dS + \int_S \tau_i\delta u_{i,j}n_j dS. \quad (21)$$

According to finite element formulations the strain and stress tensors can be expressed as

$$\boldsymbol{\varepsilon} = \mathbf{B}\mathbf{v}, \qquad \boldsymbol{\sigma} = \mathbf{D}\boldsymbol{\varepsilon}, \tag{22}$$

where $\mathbf{B}$ is the matrix containing linear combinations of the first derivatives of the shape function matrix components, while $\mathbf{D}$ is isotropic elastic constitutive matrix. Analogously to (22), the strain gradient tensor is introduced as

$$\boldsymbol{\varepsilon}_{,1} = \begin{pmatrix} \varepsilon_{11,1} \\ \varepsilon_{22,1} \\ \varepsilon_{12,1} \end{pmatrix} = \mathbf{B}_{xx}\mathbf{v}, \qquad \boldsymbol{\varepsilon}_{,2} = \begin{pmatrix} \varepsilon_{11,2} \\ \varepsilon_{22,2} \\ \varepsilon_{12,2} \end{pmatrix} = \mathbf{B}_{yy}\mathbf{v}, \tag{23}$$

where matrices $\mathbf{B}_{xx}$ and $\mathbf{B}_{yy}$ contain linear combinations of the second derivatives of the shape function matrix components with respect to x and y, respectively. Using (23) and by means of (15), the expressions for the double stress tensors are obtained as

$$\boldsymbol{\mu}_{1ij} = \begin{pmatrix} \mu_{111} \\ \mu_{122} \\ \mu_{112} \end{pmatrix} = l^2\mathbf{D}\boldsymbol{\varepsilon}_{,1}, \qquad \boldsymbol{\mu}_{2ij} = \begin{pmatrix} \mu_{211} \\ \mu_{222} \\ \mu_{212} \end{pmatrix} = l^2\mathbf{D}\boldsymbol{\varepsilon}_{,2}. \tag{24}$$

Finally, substitution of (19) and (22) – (24) into (25) yields the following well-known finite element equation

$$\mathbf{K}\mathbf{v} = \mathbf{F}\,. \tag{26}$$

In equation (25), the element stiffness matrix $\mathbf{K}$ is defined as

$$\mathbf{K} = \mathbf{K}_l + l^2\left(\mathbf{K}_{xx} + \mathbf{K}_{yy}\right), \tag{27}$$

where

$$\mathbf{K}_l = \mathbf{B}^T\mathbf{D}\mathbf{B}, \qquad \mathbf{K}_{xx} = \mathbf{B}_{xx}^T\mathbf{D}\mathbf{B}_{xx}, \qquad \mathbf{K}_{yy} = \mathbf{B}_{yy}^T\mathbf{D}\mathbf{B}_{yy}. \tag{28}$$

The nodal force vector has the following form

$$\mathbf{F} = \int_S \left[\mathbf{N}^T\mathbf{t} + \left(\mathbf{n}_1\mathbf{N}_{,1}^T + \mathbf{n}_2\mathbf{N}_{,2}^T\right)\boldsymbol{\tau}\right]dS. \tag{29}$$

As may be observed from Eq. (30), , the stiffness matrix of the strain gradient element consists of the two parts: basic ($\mathbf{K}_l$) and higher order one ($\mathbf{K}_{xx}$ + $\mathbf{K}_{yy}$). Besides, when the length parameter l is set to zero this equation is reduced to the classical one.

3.5 Verification

The finite element C1PS3 described above is implemented into the ABAQUS FE program via the user element subroutine (UEL). To examine the performance of the element, the numerical examples presenting the patch tests are performed, where the cantilever beam subjected to bending is considered. This test is used to assess the sensitivity of the element C1PS3 to geometric distortions and FE mesh is taken from [9], as shown in Fig. 3. As can be seen, this patch test is originally intended for the quadrilateral elements, and then the default discretization is adjusted to the triangular finite elements, as presented in Fig. 4.

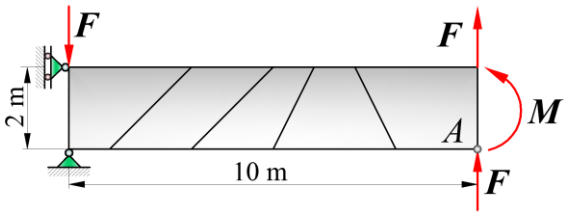

Figure 3. A cantilever beam subjected to bending

Two loading cases are studied. The first one is the case with the linear bending caused by the concentrated forces (F =150 N), and the another one is the case with the pure bending caused by the bending moment (M = 2000 Nmm).

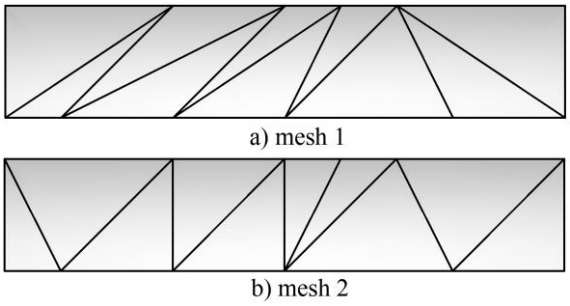

Figure 4. Discretization of a beam by triangular finite elements, a) mesh 1, b) mesh 2

The elasticity modulus and Poisson's ratio of the beam are 1500 MPa and 0.25, respectively. The vertical displacement at point

A of the presented C1PS3 FE is compared with the displacements obtained by the triangular and quadrilateral plane elements from the ABQUS library. For each load case the analyses are performed with the 5 different element types: CPS4 (four-node quadrilateral), CPS8 (eight-node quadrilateral), CPS3 (three-node triangular), CPS6 (six-node triangular) and finally C^1 triangular element C1PS3 described in this paper.

The finite elements from ABAQUS library are standard C^0 elements with two degrees of freedom per node, i.e. displacements in *x* and *y* directions. To impose the boundary conditions for the strain gradient C1PS3 element, except displacements, it is necessary to define their first and second derivatives. The first derivatives of both displacements are left free, while all second derivatives except the second derivative of *y* displacement with respect to *x* are constrained. The results of the vertical displacement at point *A* for the two load cases considered are compared with the exact reference solution taken from [10] in Tables 2 and 3.

From the results presented it can be clearly seen that the element C1PS3 passes the patch test and consequently it can be applied for the modelling of strain gradient problems. The results obtained by the mesh 1 show a stiffer element behaviour due to the excessive mesh distortion, while the mesh 2 gives very good results for both types of load. In addition, it is shown that in contrast to the parabolic elements, the linear elements from the ABQUS library can not satisfy the considered patch test.

Table 1. Vertical displacement at point *A* for point loads

	Vertical displacement of *A*, mm
CPS4	50.68
CPS8	101.46
CPS3 mesh 1	19.8
CPS3 mesh 2	30.4
CPS6 mesh 1	100.39
CPS6 mesh 2	101.3
C1PS3 mesh 1	99.78
C1PS3 mesh 2	102
Exact [10]	102.6

Table 3. Vertical displacement at point *A* for pure bending

	Vertical displacement of *A*, mm
CPS4	45.65
CPS8	99.7
CPS3 mesh 1	16.74
CPS3 mesh 2	27.28
CPS6 mesh 1	100
CPS6 mesh 2	100
C1PS3 mesh 1	97.58
C1PS3 mesh 2	99.78
Exact [10]	100

4. Further investigations

Further study will be focused on the application of the developed computational homogenization algorithm to simulate the deformation process of the nodular cast iron EN-GJS-400-18-LT with the four different microstructures obtained by the following casting technologies: Osmosis, Flotret, Tundish and Inmould.

For the multiscale simulation, the mechanical properties of the micro-constituents (Fig. 5) will be taken from the literature [4]. Besides, based on a comprehensive metallographic analysis, the averaged microstructural characteristics will be determined to define the RVE for all investigated material types.

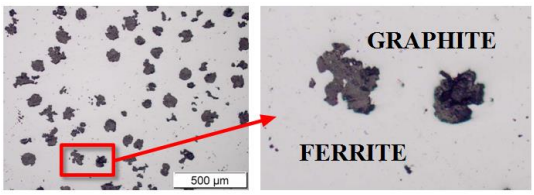

Figure 5. Nodular cast iron microstructure counterparts (Flotret process)

5. Conclusion

The paper presents the second-order computational homogenization algorithm and the strain gradient triangular finite element derived for the plane strain and plane stress problems. The FE presented and the computational algorithm are implemented into the FE program ABAQUS. The robustness of

the FE formulation is verified by using the standard patch tests.

In the further investigation the proposed numerical formulation will be used to model the deformation processes of the nodular cast iron with four different microstructures. The numerical model will be verified by comparing the numerical solutions with the experimental data.

6. References

[1] Kouznetsova, V. G.: „Computational homogenization for the multiscale analysis of multiphase materials“, PhD, TU Eindhoven, 2002.

[2] Miehe, C., Koch, A., „Computational micro-to-macro transitions of discretized microstructures undergoing small strain“, Archive of Applied Mechanics 72 (2002), 300-317.

[3] Geers, M., Kouznetsova, V., „Scale transitions in solid mechanics based on computational homogenization“, lecture notes, Eindhoven University of Technology.

[4] Čanžar, P., Tonković, Z., Bakić, A., Kodvanj, J., „Experimental and Numerical Investigation of Fatigue Behaviour of Nodular Cast Iron“, Key Engineering Materials 488-489 (2011), 182-185.

[5] Dasgupta, S., Sengupta, D.: „A Higher Order Triangular Plate Bending Element Revisited“, International Journal for Numerical Methods in Engineering, vol. 30, 419-430, 1990.

[6] ABAQUS 6.10.1, Dassault Systemes.

[7] Akarapu, S.: „Numerical Analysis of Plane Cracks in Strain Gradient Materials“, Master Thesis, Washington State University, 2005.

[8] Hahn, H. G.: „“Methode der finiten Element in der Festigkeitslehre“, Akademische Verlagsgesellschaft Wiesbaden, 1982.

[9] Rezaiee-Pajand, M., Yaghoobi, M.: „Formulating an effective generalized four-sided element“, European Journal of Mechanics A/Solids 36 (2012) 141-155

[10] Cen, S. et al.: „Quadrilateral membrane elements with analytical element stiffness matrices formulated by the new quadrilateral area coordinate method“, QACM-II. Int. J. Numer. Meth. Eng. 77, 1172-1200, 2009.